J Neurophysiol 135: 852–864, 2026.
First published March 2, 2026; doi:10.1152/jn.00467.2025

american physiological society

JNP JOURNAL OF NEUROPHYSIOLOGY

RESEARCH ARTICLE

Neural Circuits

Selective genetic targeting of the mouse efferent vestibular nucleus identifies monosynaptic inputs and indicates function as multimodal integrator

Miranda A. Mathews,[1]* Victoria W. K. Tung,[1]* Emily C. Reader-Harris,[1,2]* and Andrew J. Murray[1]*

[1]*Sainsbury Wellcome Centre for Neural Circuits and Behaviour, University College London, London, United Kingdom and*
[2]*School of Biomedical Sciences, Faculty of Biological Sciences, University of Leeds, Leeds, United Kingdom*

Abstract

The vestibular system is a critical sensory modality required for coordinated movement, balance, and our ability to interact with the surrounding environment. Vestibular sensory neurons provide the nervous system with information about head rotation and acceleration. However, the nervous system can also modify the activity of sensory neurons and hair cells via the actions of the efferent vestibular system (EVS). The function of the EVS has remained unknown partly because of an inability to target efferent vestibular neurons in a selective manner to understand their synaptic inputs and function during behavior. Here, we present a novel method for the selective targeting and expression of flp-recombinase in EVS neurons. We take advantage of the dual expression of choline acetyl transferase (ChAT) and calcitonin gene-related peptide (CGRP) in these neurons to develop an adeno-associated virus (AAV) that expresses a gene only in neurons with this intersectional expression. We use this system to map the monosynaptic inputs to EVS neurons and show inputs from distinct populations of brainstem and midbrain regions, indicating a functional role as a multimodal processing center and integrator for the vestibular periphery. To demonstrate the applicability of our technology in behavioral assays, we performed a preliminary behavior analysis (treadmill running and open field) in mice with disrupted EVS function. Although more bespoke assays are required to ascertain EVS function(s), our viral method presents a novel tool for investigators examining the role of the vestibular system and its central circuits.

NEW & NOTEWORTHY We provide a novel means of targeting and accessing the EVN and provide valuable new information on the anatomical organization of the efferent vestibular system. For the first time, we present a holistic understanding of the type of information that the EVN receives and processes, highlighting the multimodal nature of the EVN, acting as a hub to update the vestibular periphery in real time with relevant internal and external information to support overall vestibular health.

CGRP; efferent vestibular nucleus; monosynaptic rabies tracing; sensory systems; viral targeting

INTRODUCTION

The vestibular system is indispensable for the coordination of movement, balance, and our general ability to interact with the environment. This "sixth sense" provides information regarding head rotation and acceleration, which is combined in the brain with other sensory modalities to give a sense of the position and movement of the body in space.

Anatomically, vestibular organs for all land vertebrates are in the inner ear, and vestibular sensory neurons relay information to the brainstem. Aquatic vertebrates possess an additional system, the lateral line, that detects changes to the surrounding aquatic environment (such as pressure, vibration, and movement) and is critical for orientation underwater. Like several sensory systems, communication is bidirectional, where the central nervous system can exert influence over the peripheral sensory organs. A central modulation of vestibular end organs has been observed across all vertebrates, and is termed the efferent vestibular system (EVS). The EVS originates in the efferent vestibular nucleus (EVN) of the brainstem, and EVN neurons terminate directly on vestibular hair cells and afferent sensory neurons. In amphibians, efferent fibers innervate both the inner ear and

*M. A. Mathews and V. W. K. Tung contributed equally to this work. E. C. Reader-Harris and A. J. Murray contributed equally to this work.
Correspondence: M. A. Mathews (ma.mathews232@gmail.com); E. C. Reader-Harris (ec.reader-harris@leeds.ac.uk).
Submitted 3 October 2025 / Revised 5 November 2025 / Accepted 22 February 2026

lateral line (1). However, although we know the EVS has specific cellular actions on vestibular and lateral line sensory receptors (for reviews, see Refs. 2 and 3), a specific behavioral and functional role is yet to be understood.

Over the last seven decades, researchers have adapted a variety of in vivo and in vitro techniques to understand the function of this small and evolutionarily conserved nucleus. These experiments fall into three broad categories: *1*) EVS stimulation [e.g., chemically, electrically or thermally (most recently in Ref. 4) combined with recording peripheral vestibular activity (summarized in Ref. 2)]; *2*) putative physiological EVN recordings under different behavioral paradigms (some examples include Refs. 5–9); and *3*) mouse transgenic lines combined with behavioral recordings (10–13). Collectively, these works give insights into the potential function of the EVS (for reviews, see Refs. 3, 2, and 14–16), especially when paired with direct physiological recordings of EVN neurons (17, 18). However, a complete understanding of EVS function requires an ability to target and manipulate EVN neurons in awake behaving animals—which so far has not been possible.

Recombinase mouse lines, where cre or flp is expressed in genetically defined neurons, have revolutionized our understanding of behavioral roles of neuronal subtypes. In the EVN, which is a cholinergic nucleus, Lorincz et al. (19) used a ChAT-cre mouse line to perform anatomical tracing of EVS neurons. However, cholinergic neurons are widespread in the brain and perform multiple functions, so behavioral assessment of EVS function requires a finer scale of neuronal subtype resolution. Similarly, short enhancer or promoter sequences can be used within viral vectors such as adeno-associated virus (AAV) to drive cell-type-specific gene expression. In addition to ChAT, calcitonin gene-related peptide (CGRP) is known to be expressed in EVN neurons (18). Several groups have described CGRP promoter fragments for use in sensory or central neurons (20–23), providing an opportunity to utilize these same sequences for EVN targeting.

Here, we combine the ChAT-cre transgenic mouse line with both cre-dependent AAVs and a cell-type-specific short promoter to intersectionally target brainstem neurons expressing both ChAT and calcitonin gene-related peptide (CGRP). This intersection permits selective targeting of EVN neurons, which co-express both ChAT and CGRP (18, 24). We first validated this approach by retrograde labeling of EVN neurons by applying fluorogold to the end organs. Following this validation, we were able to use this novel approach to identify the monosynaptic inputs to EVN neurons using modified rabies virus (RABV) and separately block neurotransmitter release from the EVN through the directed expression of tetanus toxin light chain (TeLC). This approach demonstrates that the EVN can be selectively targeted, providing a novel tool to further explore the role of the EVS in gross motor and vestibular coordination.

MATERIALS AND METHODS

Generation of AAV Constructs

AAV constructs using the CGRP short promoter were based on a promoter sequence from Durham et al. (22) and Thomas et al. (25). We de novo synthesized (GeneArt, Life Technologies) a 2Kb region immediately upstream from the CGRP-β coding region. The sequence of the promoter region is as follows:

5′ ACGCGTGGTACCCCTGCCAGCTGTCGGATGCCTGAA-
CCTATGGATGCTTAACCAGCAGCTGAGTGAGTGTGAAAG-
TTCCCTGCTGACCCCTGGGTTGCTCAGGTGGCCTGTGCAG-
GACCCTGGCTCAGCTCTCAAGCTCTGCAGAGTGGGGTGGT-
GGAGATGCAGGGGAGGGGAAGGGAACTGCCATCTGAGCG-
CCAGCCTCCTGCTAGGCAAACCCGCCAGGGATGCTTGGAA-
GTGCTTTAATCTACACTGCTACAGCAGTGTGAGGTCTGGG-
GATTTGAATGGGGGCGGGGGAGGGATGTAAAAACCATAG-
CGCAGGATTTGGAAGGTCTGGTACAGGAGGAGAAAGCCC-
AGTTCCCTGTGCAGTCTGTTAGCCTGCTGCTCCACAATAC-
TCTCTAGTTTCTATCCTTATTAGGTGATGGGAAGCACGCA-
CTGCTAGAGTGCCCATTTGGGACAGGTATGACAGAAGTA-
CCCTAATGTATCCAAGGACCCGCTTCTTCCTGTGACAGTC-
ATCATCGTGGATGTATCTACTGAAGTCCTTTTAGAACCTG-
GGAGTGCTACTCAGCCTGCGTGGGAGTCCAGCTACGAGG-
TTCAGGTCCCCATTGGAGTGGGCAGCAAAAGGTTGTAGG-
CTGGAGTTCAGGTATTAAAGAGGTCGTGATGTCAAACTC-
AGGTTTGCTCACATTCTGGACGAATTCACCCTCTCTGTAT-
CCTTACCCCACCCCCACTCCCACTCCTACCCGGTTCCTCAG-
CAATGACCTCAAAGACAGGGAGTGGACTGCTGCCTCCCTC-
CTGCAGAAGTGTAAGTAGCTCCAGCTATGACGTTATGGA-
AGCTCGGTCAGAGCTCTGATTGGTGGAAGAGCTACTGCG-
GACCCCCCACACCCTCAAGATCGAGAATAAGAGACCACG-
GCTCTGGGGACAAGACGCCTACAGCCGTGTGTGTGTGCTC-
TTCTGCAGTGGACACTTCACTCTCGCTGTTCCAACACGGG-
CTAGCAGGTGAGAAACTTAACTTCTCAACGCCTACAGCTC-
TCTCTCCTTTAGTTTGTTTCCTTTTGGTTGCTCTTTTTAAT-
GCAGTATTTCACACTGTAGTCTAAGTTGGCCTGGCACCCA-
CTATATAGCTCAAGTTGGTTCGTCTCAAACGCTAAGGTTC-
TCCTTTCTCAGCATCCTAAGGATGCGGATTACAGGCGCAA-
GCCACCACACCCCACTCTACTTGGATCCCTTTGCTGTCCT-
GGTTCCTTATCATTCCACATACATTTCCGCCTTCCTGCAG-
CCATTGTCAGAAAGTACAGTCTTGACATTTTCTTTTAACT-
AAAGTAAGTGGGACCCCTACGACTACTCAGCAGCACTGG-
AAGCTGGGCGACCCTATCTAGGCGCGTCTGTGCCCCCTCC-
TTGAGGGAAGGTGGTCTTGCCGCATCCTAACCAGTTTTAG-
GTTAAAGAGTTCCTTGGATTCGGGATTGGGGAGCACTGA-
TCTTTTCTCTCAGATGTTTCCAGCCTTTAGCCTCCTGGGG-
TTATCAGCAAGCAGGTGGGTCTCGCTTCGCTGTGGGGAG-
GAGGAGTCCTCATCTGCGGTTCTGAGGTAGTTTAAAAAA-
AAAAATCTCCCAACTCTGCAGATGGAGAGAGGGGGATTA-
GTTCCAAGTTAACTTTCTTCCCCAGGGCAACCTCTCAGAA-
AGGGTGATTATAATAATTTCAACCTGTTAGAAATCCTTAG-
CAGCGGGACAGCAAGGCGCAGGGATCTCTGGGTGGTTTT-
TGGTTTCTTCACAGATGAGAGCCAAAGGGGCGCGGCACG-
TGTGTTCTCCTGCAAGCTGGGGGCAAATGAGTGCCGGTA-
GCTCCTCCTTGTTCTTAAACCGAGCAGAAACTGCAAACCA-
CATCTACTCTCCCCCACTCGTTTCTGCTCTATCAAGCCACT-
CACCACACTGCATCTACTGCACGTTTTGAGAGCTGCAGTG-
TGGTAGGAGAAATAGAACCTGGGTCTATAGTCCTGAGCA-
ATTGGACCATTCTTCTCTTCTTACAGAGACATCTTAATTA-
ACTAGTGCGGCCGCCACCTCTAGAGGATCC 3′.

The vector pAM-CGRP-FLPo-HA was used for initial testing of the CGRP promoter. DNA was de-novo synthesized containing the entire 2Kb CGRP promoter region upstream from FLPo, a 2 A self-cleaving peptide sequence and 3× HA tags. This entire sequence was cloned into a

vector containing AAV2 inverted terminal repeats (ITRs) (26) via KpnI and HindIII restriction sites.

The CGRP and cre-conditional FLPo or GFP (pAM-CGRP-Flex-FLPo or pAM-CGRP-Flex-GFP) were generated by replacing the CAGGS promoter in pAM-Flex-Empty (a cre-conditional vector containing AAV2 ITRs; 26) with the CGRP short promoter via KpnI and XbaI restriction sites. FLPo or GFP was cloned in reverse orientation into the multiple cloning site using EcoRI and XhoI restriction sites.

Generation of Recombinant AAVs

AAV vectors used in this study were all packaged according to McClure et al. (27) with some minor modifications. Briefly, human embryonic kidney (HEK) 293 cells were transfected via either calcium phosphate or Turbofect (Thermo Fisher Scientific) with individual AAV backbone plasmids as well as a 1:1 ratio of AAV1 (pH21) and AAV2 (pRV1) or AAVDJ helper capsid proteins and adenovirus helper plasmid pFdelta6. 48 h post-transfection, the cells were harvested and AAVs purified using 1 mL HiTrap heparin columns (Sigma), concentrated using Amicon Ultra centrifugal filter devices (Millipore), and purified using an AAVpro Purification Kit (Takara Bio).

The recombinant AAVs we designed and produced for selective EVN targeting were, in order of experimental use:

1) AAV[2/1]-CGRP-FLPo-HA
2) AAV[DJ]-CGRP-FLEx-GFP
3) AAV[DJ]-CGRP-FLEx-FLPo

Other AAV vectors used in this study were:

- AAV[DJ]-Ef1a-frt-H2BG-TVA (for rabies monosynaptic tracing; 28)
- AAV[DJ]-Syn-frt- H2BG-N2cG (for rabies monosynaptic tracing; 28)
- AAV[DJ]-EF1a-fDIO-TeLC-GFP (for behavioral recordings after blocking EVN transmission; ETH Zurich Vector Core)
- AAV[DJ]-EF1a-fDIO-GCaMP6s (control for behavioral recordings with TeLC injections; Addgene plasmid #105714).

Animals

All animal experiments were performed under UK Home Office license (PPL: PE4FA53CB) according to the United Kingdom Animals (Scientific Procedures) Act 1986. Male and female mice aged between 8 and 16 wk old from C57BL/6J and B6J.ChAT-IRES-cre::Δneo (ChAT-cre; JAX Stock No.: 031661; 29) homozygous animals were used for experiments.

Initial experiments used ChAT-cre::tdTomato mice that were generated in-house from a cross between homozygous strains B6J.ChAT-IRES-cre::Δneo and ROSA-loxP-STOP-loxP-tdTomato (30). These mice expressed tdTomato exclusively in cholinergic neurons and were used to demonstrate the location of EVN neurons (ChAT-positive) with peripheral fluorogold labeling.

All animals were housed in a temperature-controlled environment with a 12 h light/dark cycle (red lights on at 0900) and free access to food and water. Surgeries and behavioral experiments were carried out during the dark phase of the cycle. All efforts were made to minimize animal suffering.

Surgical Procedures

Stereotaxic injections.

Stereotaxic injections into the EVN were made as described previously (26), adapted from Cetin et al. (31). Briefly, mice were anesthetized with isoflurane in oxygen (4% induction; 2% maintenance during surgery) and given a subcutaneous injection of analgesics (Metacam at 5 mg/kg). The mouse was fixed in a stereotaxic frame (Model 942, Kopf, USA), and an incision was made in the skin such that bregma and lambda could be exposed and visualized. A small burr hole was made above the injection site (relative to bregma) where viruses were injected using a pulled 3.5 in. borosilicate glass capillary with 8 μm bore width (Cat. no.: 3-000-203-G/X; Drummond) and Nanoject II or Nanoject III (Cat. No.: 3-000-207 and 3-000-204, respectively; Drummond). Stereotaxic coordinates relative to bregma for specifically targeting the EVN were as follows: anterior/posterior −5.80 mm; lateral +0.60 mm; depth from brain surface −4.4 and −4.3 mm. Each depth received 100 nL of AAVs or 200 nL of rabies (CVSN2c-ΔG-EnvA-mCherry, Sainsbury Wellcome Center Virology Core Facility), depending on the surgery. Following viral injection, the skin was closed with sutures (Cat. No.: VR493; Ethicon).

Subsequent rabies injection or histology began no sooner than 14 days after the initial injection of AAVs to allow sufficient time for their expression. Likewise, histology following rabies injections also took place 14 days after rabies injection for the same reason.

Retrograde labeling.

To identify EVN neurons, fluorogold was injected into the right horizontal semicircular canal of ChAT-cre::tdTomato or Chat-cre mice. These retrograde injections were made as described previously (18). Briefly, mice were anesthetized with 4% isoflurane in oxygen, given appropriate analgesics, and maintained on 2% isoflurane in oxygen during surgery. The area behind the ear was shaved and cleaned, and an incision was made 1 mm behind the right pinna. The muscles were separated such that the horizontal semicircular canal was visualized. A 23-G needle was used to thin the bone of the horizontal semicircular canal until a small hole (∼100 μm) was made. A 29-G needle attached to a 1 mL insulin syringe was used to carefully introduce 100 nL of 2% fluorogold (Sigma-Aldrich) in saline into the horizontal canal, and the skin was sutured. Animals were sacrificed 3 days later by transcardial perfusion, as described below.

Tissue Preparation and Histology

Mice were deeply anesthetized with intra-peritoneal injection of pentobarbital (200 mg/mL concentration at 10 mg/kg dosage; Dolethal) and subsequently transcardially perfused with 0.1 M phosphate buffer saline (PBS, pH 7.4) followed by 4% paraformaldehyde in 0.1 M PBS. The brains were harvested and immersion-fixed in 4% paraformaldehyde in 0.1 M PBS for a minimum of 2 h at room temperature. Then, 50 μm thick coronal brain sections were sliced on a Leica V1200 vibratome and collected and stored in tissue culture wells filled with 0.1 M PBS and 0.01% sodium azide solution until use.

Free-floating sections were incubated in primary antibodies diluted in 0.1 M PBT (0.1 M PBS with 0.1% Triton X-100 and 1% BSA) overnight. They were then washed three times in 0.1 M PBS for 10 min each before secondary antibody incubation (diluted in 0.1 M PBS) for 2 h. After washing again three times with 0.1 M PBS for 10 min each, the sections were mounted onto Superfrost + (Thermo Fisher Scientific) glass slides, dried, and cover-slipped with DAPI-Fluoromount (SouthernBiotech 0100-20). Primary and secondary antibodies used for different AAV and rabies surgeries are summarized in Table 1. All sections were imaged using the Zeiss AxioScan Z1 slide scanner or Zeiss AxioImager at ×10 or ×20 magnification.

Cell Counting

Manual.

For monosynaptic rabies tracing, the cell numbers of "starter" EVN neurons (defined as expressing both the nuclear GFP from the AAV and mCherry from the RABV) were determined by eye, focusing through 50-μm-thick coronal sections containing the EVN and counting the nucleoli identified with DAPI staining in consecutive sections containing the EVN.

QUINT workflow.

In rabies tracing experiments where manual cell counting was not practical, cells were quantified and spatially analyzed in a semi-automated manner using open-source software in QUINT workflow (detailed in Ref. 32). Briefly, serial sections were registered to a three-dimensional (3-D) reference atlas (Allen Brain Mouse Atlas 2017) using QuickNII software. These sections are then segmented into cell, tissue, and background using the ilastik software. Finally, Nutil software was used to merge custom atlas maps from QuickNII with segmented images from ilastik to quantify cells and their coordinates. These data were exported to Microsoft Excel for further analysis. All output cells and their locations were cross-checked against original JPEG images of sections to ensure accurate counting and location reporting—here, mislabeling was manually adjusted. Importantly, the Allen Brain Mouse Atlas 2017 used in QuickNII does not include the location for the EVN, and so EVN cells were misplaced as medial vestibular nucleus (MVN) neurons. These were manually adjusted in postprocessing.

Behavior Recording and Analysis

Behavioral assessment of TeLC expressing and control mice behavioral recordings took place at 7, 10, and 14 days post-AAV surgeries (see vectors listed earlier for details).

Open field.

Mice were allowed to freely explore a square white Perspex arena for a period of 5 min while being recorded by an overhead Doric Behavior Tracking video camera recording at 30 frames per second. To avoid the effects of habituation on experiments, mice were exposed to the arena for 5 min on the 3 days before experimental recordings.

Videos were analyzed in EthoVision XT (Noldus) video tracking software. Here, center-point tracking feature was used to track and generate total distance traveled as well as heat maps of movement where pixel color represents total time spent at the location (more time spent corresponds to lighter blue color). Distance travel data were exported to Microsoft Excel for plotting and further analysis. TeLC and control conditions were compared using the Student's paired *t* test.

Balance beam.

The balance beam test (adapted from Ref. 33) was used to measure subtle motor changes in mice where EVN transmission was blocked. The beam (1 cm^2; 83 cm in length) was elevated and suspended between two platforms of different heights (13 cm on the left and 19 cm on the right) to create a slight incline of 3°. On the right-hand side, the platform included a stage for mice to walk to and rest. A mirror was placed below and angled so as to reflect the underside of the beam and mice onto the video recorder. Mice were habituated and trained to walk on the beam before AAV injections by placing the mouse progressively further away from the end platform and stage. Video recording from the right-side view of the mouse was carried out with a high-speed camera (Ximea), recording at 200 frames per second.

Videos were analyzed in MaxTraq Software (Innovision Systems) for the speed of traversing across the beam and the nose-to-tail angle of each mouse measured at the center of the beam. Tracking data were exported to Microsoft Excel for plotting and further analysis. TeLC and control conditions were compared using the Student's paired *t* test.

RESULTS

Molecular Targeting of EVN Neurons

EVN neurons are known to co-localize ChAT and CGRP in mice (18, 24). We used this information to design an intersectional genetic strategy to selectively target these neurons via a stereotaxic injection into the brainstem. First, we anatomically visualized EVN neurons, which are known to project and synapse onto vestibular hair cell receptors and primary afferents in the peripheral sensory apparatus, by injecting

Table 1. *Antibodies used throughout for immunohistochemistry experiments*

Experiments	Primary Antibody (Dilution, Catalogue Number)	Secondary Antibody (Dilution, Catalogue Number)
Figure 1	Chicken anti-GFP (1:1,000, AB13970)	Anti-Chicken 488 (1:1,000, A11039)
	Rabbit anti-FG (1:200, AB153-I)	Anti-Rabbit 594 (1:1,000, A21207)
Figure 2	Mouse anti-mCherry (1:1,000, AB125096)	Anti-Mouse 594 (1:1,000, A21203)
	Sheep anti-ChAT (1:250, AB18736)	Anti-Sheep 647 (1:1000, A21448)
Figure 3	Chicken anti-GFP (1:1,000, AB13970)	Anti-Chicken 488 (1:1,000, A11039)
	Rabbit anti-TeLC (1:1,000, AB53829)	Anti-Rabbit 647 (1:1,000, A21245)
	Chicken anti-GFP (1:1,000, AB13970)	Anti-Chicken 488 (1:1,000, A11039)

the retrograde tracer fluorogold into the horizontal semicircular canal of ChAT-cre::tdTomato mice.

Fluorogold labeling of EVN neurons, which are located dorsolateral to the genu of the seventh cranial nerve, was observed overlapping with ChAT-positive putative EVN neurons, confirming that EVN neurons can be targeted using cholinergic labeling in ChAT-cre animals (Fig. 1*A*). However, cholinergic neurons are also observed in the nearby abducens nucleus, limiting the ability to target the EVN with stereotaxic injections alone. We therefore attempted to further refine this targeting by complementing the cre line with an AAV that only expressed a transgene in neurons that were both ChAT (cre) and CGRP positive. This AAV used a CGRP promoter fragment to express a nuclear-tagged human influenza hemagglutinin (HA) in CGRP-positive cells. We used this in combination with a cre-dependent AAV to express GFP in ChAT-positive cells in ChAT-cre mice. Stereotaxic coinjections of both AAVs in ChAT-cre mice allowed us to visualize ChAT-positive cells in green and CGRP-positive cells in red. We observed co-localization of GFP and HA in EVN neurons (Fig. 1*B*).

Next, we developed a cre-dependent AAV using this CGRP promoter to selectively express GFP in cells that are both ChAT and CGRP positive. Stereotaxic injections of this AAV allowed us to visualize GFP in EVN neurons. To ensure the AAV effectively targeted EVN neurons, we performed fluorogold injections in the horizontal semicircular canal according to anatomical localization described in Schutz et al. (34). Co-localization of GFP with fluorogold was observed on average (± standard deviation) in 15 ± 4 neurons ($n = 5$ animals), representing ∼40% of the nucleus, confirming this strategy selectively targets EVN neurons (Fig. 1*C*).

Monosynaptic Inputs to EVN Neurons

Selective expression of recombinases, such as flp recombinase, in genetically defined neurons provides a means to interrogate both their anatomy and function (35). Our intersectional approach provided a means to selectively target EVN neurons, and therefore, we developed a viral vector (pAAV-CGRP-FLEx-FLPo) that combined the short CGRP-promoter and cre-conditional expression to drive flp-recombinase only in EVN neurons (Fig. 2*A*). We first used this tool to identify direct synaptic inputs to EVN neurons.

We co-injected a mixture of three AAVs into ChAT::cre mice – AAV[DJ]-CGRP-FLEx-FLPo to drive selective FLPo expression only in EVN neurons, and AAV[DJ]-Ef1a-frt-H2BG-TVA and AAV[DJ]-Syn-frt-H2BG-N2cG to express the TVA receptor and rabies glycoprotein, respectively, in a flp-recombinase dependent manner. The TVA receptor permits selective cell entry of EnvA-pseudotyped rabies virus, while rabies glycoprotein expression enables monosynaptic transfer of rabies virus (28). Two weeks following this AAV injection into the region of the EVN, we injected RABV-N2c-EnvA-mCherry at the same stereotaxic coordinates to target EVN neurons and identify their monosynaptic inputs (Fig. 2*B*).

We identified five starter EVN neurons across three mice. These starter neurons were abundantly innervated from input regions (starter to input neuron ratio of 1:356). Almost all monosynaptic inputs to EVN neurons were found within the brainstem/midbrain region (such as vestibular nuclei, reticular formation, medullary and pontine regions, and autonomic/arousal nuclei), suggesting modulation by local circuits (Fig. 3*A*). No neurons were observed in cortical or thalamic regions, or in the spinal cord (data not shown). Details of all input sources and distribution are presented in Supplemental Tables S1 and S2.

The small number of EVN starter neurons provides the opportunity to assess the heterogeneity of inputs to different EVN cells. To assess the consistency of presynaptic inputs to the EVN, we compared the identity and relative contribution of input sources across animals (Fig. 3*B*) and applied statistics on all animal pairs (1034596 vs. 1034597, 1034596 vs. 1034598, 1034597 vs. 1034598). We observed 21 unique input sources, 13 (62%) of which were shared across the three mice (Jaccard index paired scores 0.65–0.79). This suggests a core network of inputs present: the MVN, EVN, nucleus prepositus, pons, medulla, spinal vestibular nucleus, pontine central gray, sublaterodorsal nucleus, supragenual nucleus, subceruleus nucleus, paragigantocellular reticular nucleus, and superior vestibular nucleus. The MVN was the dominant input source, accounting for ∼42%–75% (normalized) of total presynaptic neurons across animals. Other shared sources contributed smaller but consistent fractions of the total input. Moreover, Pearson correlations were high across all animal pairs ($r = 0.91$–0.97), indicating strong alignment across animals in the proportional weighting of inputs. Spearman correlations were moderate to high ($r = 0.59$–0.71), reflecting a conserved ranking of dominant inputs with greater variability among lower contributing nuclei. Together, these analyses demonstrate that EVN neurons receive input from a conserved set of presynaptic sources with highly similar distributions across animals. Variability across animals primarily reflects differences in the relative contribution of minor inputs rather than changes in the core afferent architecture.

EVN Inhibition in Behavior

A complete understanding of the function of any neural circuit requires the ability to selectively alter the synaptic output of that group of neurons. To demonstrate whether our novel method could potentially be used to block synaptic output from EVN neurons, we combined the selective flp-recombinase expression described above with an AAV that drives the expression of tetanus toxin light chain (TeLC) in a flp-dependent manner (Fig. 4*A*).

TeLC is a potent means to block synaptic transmission and does so via the cleavage of the synaptic protein VAMP2, preventing vesicle docking. AAV mediated expression of TeLC is known to completely block the release of neurotransmitters with effects beginning ∼10 days after AAV injection (26).

In experimental animals, we performed bilateral co-injections of our EVN targeting AAV (AAV[DJ]-CGRP-FLEx-FLPo) with the flp-dependent AAV[DJ]-EF1a-fDIO-TeLC-GFP into ChAT-cre mice to selectively block synaptic transmission only from EVN neurons. Control animals received an injection of AAV[DJ]-EF1a-fDIO-GCaMP6s instead of TeLC at the same coordinates.

To assess whether our technique could be used to interrogate the behavioral role of EVN neurons, we performed two preliminary behavioral assays. Before formal behavioral

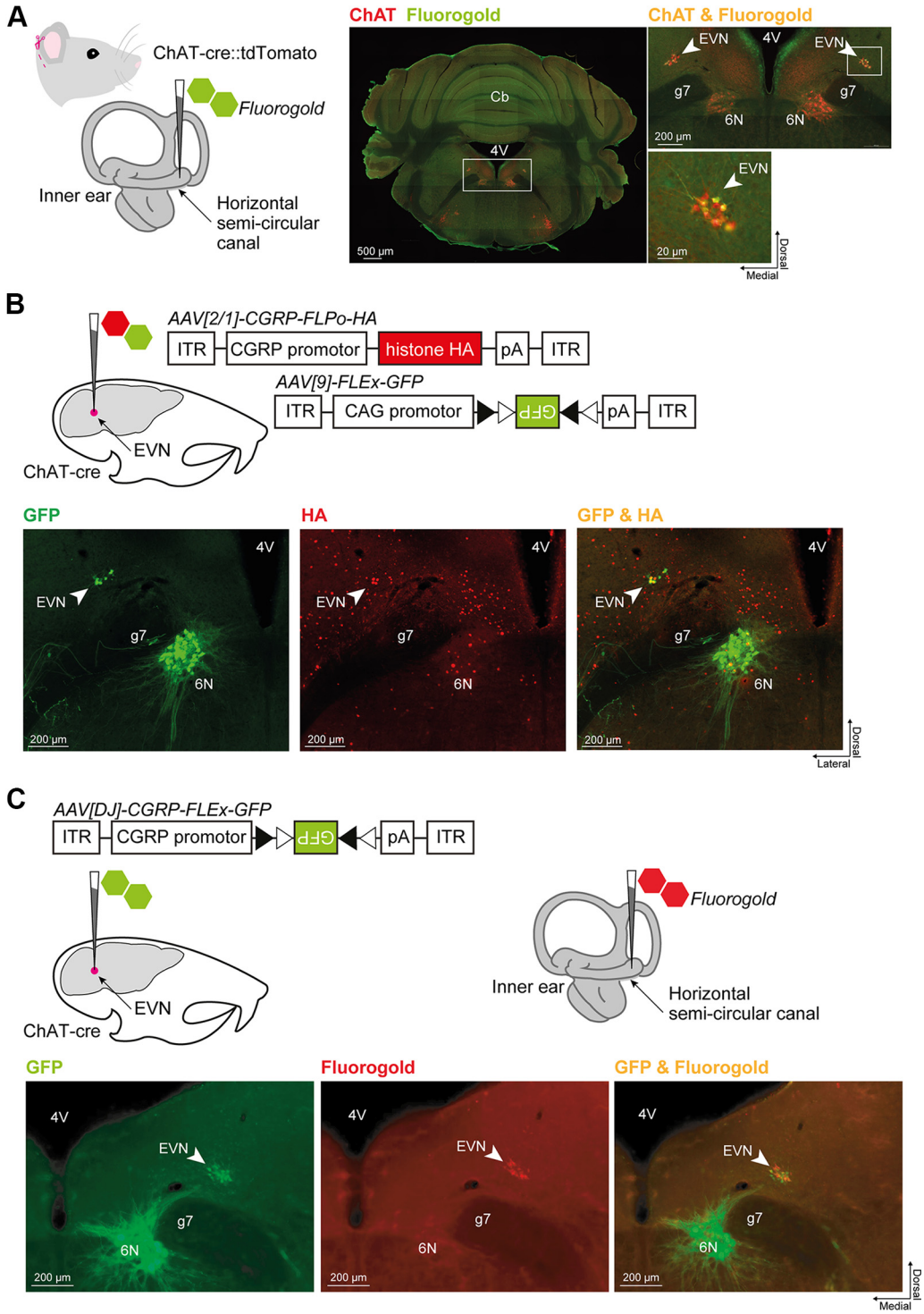

Figure 1. Molecular-genetic targeting of EVN neurons. *A*: the fluorescent retrograde tracer fluorogold (FG) was injected into the horizontal semicircular canal of ChAT-cre::tdTomato mice. Gold FG staining overlaps with red ChAT-positive, putative EVN neurons in red (arrow, insets), confirming EVN is located dorsolateral to the genu of the seventh cranial nerve (g7), and can be targeted with ChAT-cre animals. *B*: in ChAT-cre mice, a 1:1 ratio of cre-dependent AAV expressing GFP and a HA-expressing AAV (red) under control of the CGRP promoter was stereotaxically injected into the EVN. Yellow overlap (arrow, far right image) confirms that CGRP and ChAT can be used to selectively target EVN neurons. *C*: combined strategy where a single AAV combines the CGRP promoter and a cre-dependent FLEX switch can be used to target EVN neurons, confirmed by stereotaxic injection of this AAV into the EVN and fluorogold injection into the semicircular canal. GFP and fluorogold co-localization observed on average (± standard deviation) in 15 ± 4 neurons ($n = 5$ animals), representing approximately 40% of the EVN. 4 V, fourth ventricle; 6 N, sixth cranial nucleus (abducens); CAG, chicken beta-actin; Cb, cerebellum; CGRP, calcitonin gene related peptide; ChAT, choline acetyltransferase; EVN, efferent vestibular nucleus; ITR, inverted terminal repeats; pA, poly A.

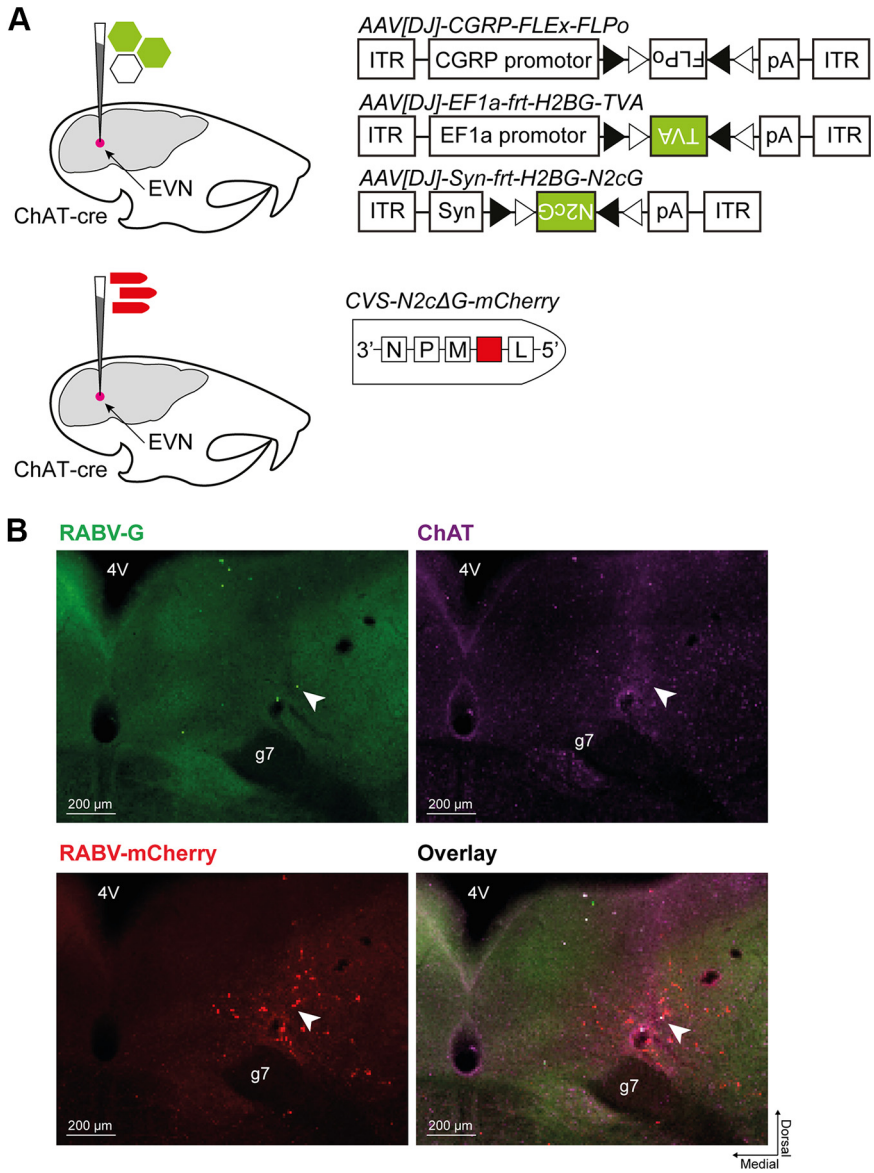

Figure 2. Monosynaptic rabies tracing of EVN neuronal inputs. *A*: strategy for rabies tracing in ChAT-cre mice where first avian receptor TVA (AAV[DJ]-EF1a-frt-H2BG-TVA) and rabies N2c glycoprotein (AAV[DJ]-Syn-frt-H2BG-N2cG) were stereotaxically injected with AAV[DJ]-CGRP-FLEx-FLPo in a 1:1:1 ratio to prime neurons for rabies tracing. Two weeks following initial rAAV injections, EnvA-psudotyped, glycoprotein-deficient rabies tagged with red fluorescent protein (EnvA-CVS-N2cΔG-mCherry) was stereotaxically injected to the same coordinates. *B*: successful transduction (arrow, overlay) of rabies glycoprotein (arrow, RABV-G) and rabies virus (arrow, RABV-mCherry) in a ChAT-positive EVN neuron (ChAT, arrow). A total of 5 starter EVN neurons were identified across 3 mice. 4 V, fourth ventricle; EVN, efferent vestibular nucleus; g7, seventh cranial nerve.

assessment, we examined animals for any gross behavioral abnormalities, especially those associated with peripheral vestibular abnormalities (36). This included tilting of the head and circling. We also examined mice for other phenotypes, such as reduced grooming and weight loss, but we did not observe any changes in these metrics (data not shown).

For a preliminary assessment of motor abnormalities in animals with disrupted EVN function, we used an open field test. Mice were tracked in an open field arena ($n = 3$ per condition) for 5 min and their path length, movement velocity, and turning velocity analyzed at 7-, 10-, and 14-days postinjection. No difference was found between control animals and those lacking EVN output (Fig. 4*B*), suggesting the EVN is not required for gross motor function.

For a behavioral assessment that would require more engagement of the vestibular system, we used the balance beam test, where animals with a vestibular impairment show balance deficits (33). As above, animals were tested 7-, 10-, and 14-days post AAV injection. Both control and EVN-disrupted animals were able to traverse the balance beam following a training period. No difference was found between groups in terms of the number of foot slips made by each animal as they walked across the beam, with both groups of animals making minimal slips per trial (foot slips per trial – day 7: control 0.4 ± 0.4, TeLC 0.5 ± 0.2; day 10: control 1 ± 0.4, TeLC 0 ± 0; day 14: control 0.5 ± 0.2, TeLC 0.17 ± 0.17).

Animals with a disrupted EVN were consistently faster at traversing the balance beam (Fig. 4*C*) (speed (cm/s) – day 7: control 6.8 ± 1.1, TeLC 8.8 ± 1.3; day 10: control 6.0 ± 1.3, TeLC 10.4 ± 0.9; day 14: control 8.6 ± 1.0, TeLC 11.8 ± 1.7). This reached statistical significance at 10 days following injection (Student's *t*-test $p = 0.021$). No other differences were found between control and EVN disrupted groups.

DISCUSSION

It is well accepted that EVN neurons contribute to fine-tuning of vestibular sensory input by modulating firing

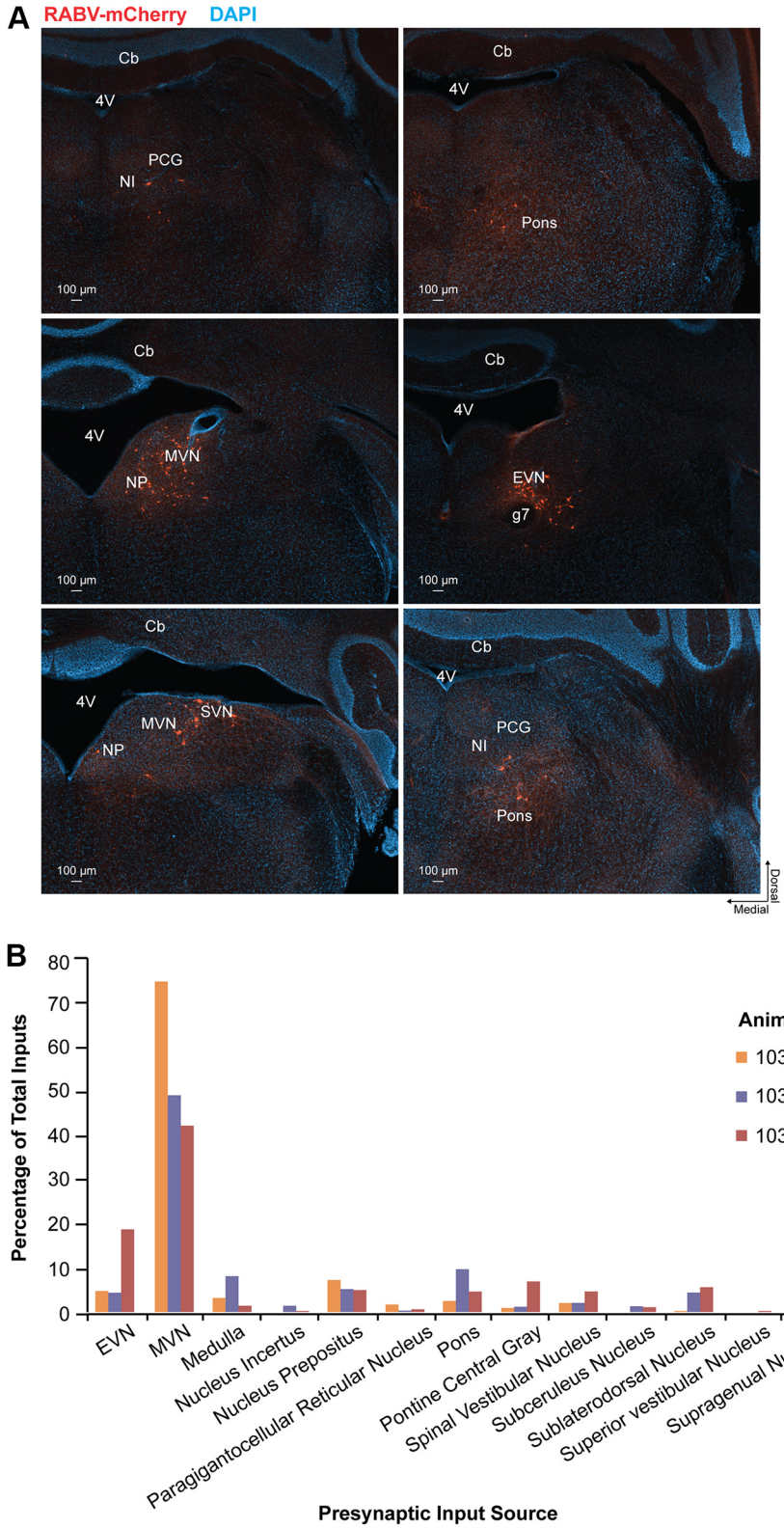

Figure 3. Identity and relative contribution of monosynaptic input sources to EVN starter neurons. *A*: example input regions from rabies tracing are shown in red. *B*: the 13 conserved input sources and their relative weighting across animals ($n = 3$) form the majority (62%) of all inputs observed. Comparing animals, Pearson correlations were high ($r = 0.91$–0.97) and Spearman correlations were moderate to high ($r = 0.59$–0.71), reflecting alignment across proportional weighting and conserved ranking of dominant inputs, respectively. 4 V, fourth ventricle; Cb, cerebellum; EVN, efferent vestibular nucleus; g7, seventh cranial nerve; MVN, medial vestibular nucleus; NI, nucleus incertus; NP, nucleus prepositus; PCG, pontine central gray; SVN, superior vestibular nucleus.

patterns, signal timing, and sensitivity of vestibular afferents and hair cells (reviewed in Ref. 14). However, the behavioral role of the EVS continues to be debated. An inability to target the EVN selectively has meant that probing its function in awake behaving animals has not been achievable. Here, we add to the toolkit for studying EVS function with a novel AAV-based EVN-targeting virus that draws on recent technological advances in neuroscience.

We combined a cre-recombinase driver line (ChAT::cre) with a short AAV promoter active in CGRP-positive neurons

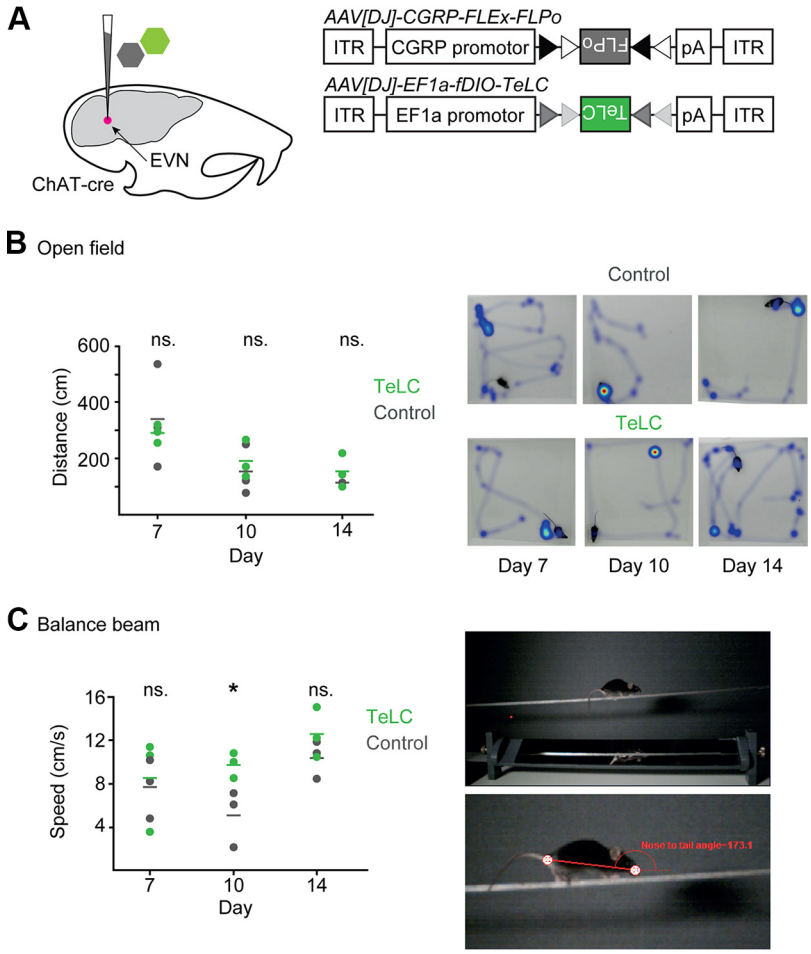

Figure 4. Selective disruption of EVN neurotransmission and behavioral assays. *A*: schematic of the strategy for selective block of EVN neurons. Tetanus toxic light chain (TeLC) was selectively expressed in EVN neurons to block their transmission in ChAT-cre mice via stereotaxic co-injection of AAV[DJ]-CGRP-FLEx-FLPo and AAV[DJ]-EF1a-fDIO-TeLC-GFP in a 1:1 ratio ($n = 3$). In control mice, TeLC was replaced with TeLC with AAV[DJ]-EF1a-fDIO-GCaMP6s ($n = 3$). *B*: no significant difference was observed across control and TeLC expressing mice in an open field (white Perspex box) arena in the first 60 seconds of recordings, measured on days 7, 10, and 14 following stereotaxic surgery. *C*: TeLC-expressing mice demonstrated a significantly faster time to traverse the balance beam than controls on day 10 following stereotaxic surgery, in line with peak TeLC activity and exposure. $*P < 0.05$.

to drive selective gene expression only in neurons that express both these genes. As EVN neurons are one of the few neuronal subtypes to coexpress these genes in the brainstem, stereotaxic injection permitted their selective targeting. We used this intersectional strategy to express a separate recombinase, FLPo, selectively in EVN neurons. Paired with recombinase-dependent AAVs, this allows for the selective anatomical mapping and activity manipulation of EVN neurons. We used this to assess direct (monosynaptic) EVN inputs and perform a preliminary behavioral assessment of EVS function. Though our anatomical and behavioral studies restricted genetic interventions to modified rabies tracing and expression of TeLC, this same system can be used for other systems neuroscience interventions, such as the selective expression of fluorescent proteins, or optogenetic or chemogenetic modulators (35) for further direct interrogation of EVS function.

EVN-Specific Monosynaptic Rabies Tracing Strategy

To date, this work represents the first monosynaptic tracing strategy selective to the EVN. We identified a small number of starter neurons (1 or 2 per animal; $n = 3$ animals). This reflects the technical challenges of targeting a very small brain region, the requirement for two stereotaxic surgeries, and the need for successful transduction by four viral vectors for a starter cell. As the precise mechanisms governing rabies virus transsynaptic transfer remain incompletely understood (37), and because low starter cell numbers can disproportionately influence estimated input fractions (38), our data set may provide only a partial representation of EVN inputs. Nevertheless, the strong alignment of input strengths (Pearson correlation 0.91–0.97 across animal pairs) and conserved ranking of input regions (Spearman correlation 0.59–0.71 across animal pairs) of our data suggests that these regions constitute a core set of EVN inputs, though there are likely additional inputs not captured by the present approach.

It is also worth noting that previously, pseudorabies virus was used to assess polysynaptic inputs to EVN neurons in gerbils (39). The number of putative starter EVN neurons reported (<6) and the distribution of inputs at early time points align with our data, with the strongest input from the MVN and reticular formation.

Direct Presynaptic Inputs Indicate EVS Function as Multimodal Processing Center

Mapping circuit architecture to function has become an important means to elucidate nervous system function. We know the EVN is sensitive to a heterogeneous input profile (18) from a variety of brain regions (39, 40), and decades of research have either demonstrated directly or hypothesized EVN activation across a wide range of behavioral and physiological conditions. By quantitatively mapping the monosynaptic inputs to EVN neurons and integrating the known functions of these source regions, we infer that the

EVN supports two distinct yet overlapping functional paradigms in vestibular efferent literature. The majority of total EVN inputs observed support *1*) vestibular plasticity and gaze stabilization (~65%) while *2*) state-dependent gating (~16%), including predictive motor suppression (~13%), represent smaller but important functions (Supplemental Table S2).

We propose that the EVN is an important component of reflexive, adaptable vestibular sensorimotor processing. Specifically, the EVN is a context-sensitive, integrative processor of vestibular, motor, and internal state information for dynamically calibrating vestibular signaling in real time. This hypothesis is consistent with the self-input we observed—the EVN likely uses an internal feedback system as an auto-tune mechanism when filtering diverse information, and accounts for the long-standing variability in EVN-linked behaviors. Further work describing the nature of these inputs (e.g., neurotransmitter phenotype) would provide more color on the context for EVN activation.

Vestibular plasticity and gaze control.

In addition to the MVN, the EVN receives input from oculomotor-associated nuclei, notably the abducens nucleus and nucleus prepositus, which are integral to horizontal gaze control and gaze holding, respectively. Collectively, these regions integrate vestibular signals with motor commands for gaze stabilization and in refining vestibuloocular reflex (VOR) gain and adaptation (41–45). Their strong input indicates the EVN aligns peripheral vestibular encoding with centrally calibrated gaze shifts. In agreement with our anatomical data, early hypotheses of EVS function included anticipation of volitional head movement and the ensuing gaze shift (46–48). Furthermore, the EVS has been suggested to have a role in vestibular plasticity, particularly regarding the vestibuloocular reflex (VOR) through signaling via alpha-9 nicotinic acetylcholine receptors (α9 nAChRs) expressed at efferent vestibular synapses on hair cells, which can elicit inhibitory responses in afferents (49–53). This plasticity could be driven by the high volume of MVN input observed in our tracing data, as electrical stimulation and lesioning of MVN neurons in rats resulted in increased expression of ChAT-positive EVN neurons (40). Alternatively, CGRP could underlie EVN activity in the VOR. CGRP knockout mice were associated with a significant reduction in the VOR sensitivity without any changes in the number of ChAT positive EVN neurons (10). Furthermore, Chang et al. (13) reported unimpaired VOR function in α9 nAChRs knockout mice, suggesting an alternative mechanism. Future work investigating the properties of MVN inputs to the EVN would help elucidate the role of the EVN in peripheral vestibular plasticity.

Separately, the EVS has also been implicated in motion sickness symptoms. CGRP expression levels increased in the EVN in rats with motion sickness (54), α9 nAChRs knockout mice with an attenuated EVN showed reduced motion sickness symptoms (55), and young adult mice displayed EVN activation (measured via cFos) during motion sickness symptoms (56). It is broadly accepted that motion sickness symptoms arise out of sensory mismatch and conflict between visual, proprioceptive, and vestibular information. EVN involvement is consistent with this model, particularly given its dense and selective innervation from brainstem and midbrain regions that integrate multimodal sensory information.

State-dependent gating.

Inputs from brainstem regions involved in arousal, visceral regulation, and motor control suggest that the EVN plays a key role in state-dependent sensory gating of vestibular input. Inputs from arousal- and sleep-related nuclei (e.g., sublaterodorsal, subceruleus, and nucleus incertus) imply that EVN activity may be modulated across sleep-wake cycles or during shifts in attentional state, potentially allowing the vestibular system to prioritize or suppress sensory input as needed (57–60). Autonomic and visceral centers, including the nucleus of the solitary tract and medullary inputs, could provide interoceptive context enabling the EVN to modulate vestibular sensitivity during challenges like nausea, hypotension, or cardiovascular changes (61, 62). Meanwhile, inputs from sensorimotor integration regions (pontine gray and supragenual nuclei) and postural control centers (spinal and lateral vestibular nuclei) support the idea that the EVN dynamically calibrates vestibular afferent output based on ongoing motor activity, body and head orientation, and valence (63, 64). Previous studies have shown EVN activity increases during aroused states in toadfish (6), and vestibular reflex sensitivity is enhanced under threatening postural conditions in humans (65, 66). Multimodal stimulation, such as light touch, sound, and visual stimuli, effectively increases EVN discharge (6, 47, 67, 68).

There is also a considerable body of literature that highlights the role of the EVN in predictive motor gating of vestibular input. In line with this, we show input from vestibulospinal and reticulospinal systems, including the pontine reticular formation and lateral vestibular nucleus (which receives both motor input directly as well as through the cerebellum; 69). These areas are central to generating motor programs for locomotion, posture, and axial control (70). Their input to the EVN could provide the route for efference copy information about impending self-motion, enabling the EVN to adjust the gain of vestibular signals during volitional movement. In fact, cholinergic efferent inhibition of hair cells at the lateral line periphery is well reported in zebrafish during swimming. In larval *Xenopus* and zebrafish, the EVS has been shown to attenuate afferent hair cell discharge in phase with locomotor activity (9, 71, 72), and in a direction-specific manner (73). In the lateral line, the EVN functions to suppress reafferent noise while ensuring sensory hair cells remain receptive to external stimuli to ultimately maintain perceptual clarity during self-generated motion. In light of the relative distribution of inputs we observed and since mammals do not possess a lateral line, it is possible that the EVN evolved to process vestibular-based input (~65%) more than motor-based input (~13%).

Behavioral Assessment of EVS Function

We performed a preliminary behavioral assessment of EVS function via the selective expression of TeLC in EVN neurons. TeLC provides a potent block of synaptic transmission ~10 days after AAV injection (26). Importantly, animals were overtly normal and showed no health problems following EVN disruption. In addition, animals showed no gross motor defects in the open field and were able to traverse a

balance beam. This latter result potentially indicates that the EVS is not required for all peripheral vestibular function, as this task is heavily dependent on the vestibular system, and mice with vestibulopathies show clear deficits in this behavior (33, 74).

Mice with a disrupted EVN did show a mild phenotype of traversing the balance beam faster than control animals. This counterintuitive result (as you may expect that animals with a suboptimal vestibular system would be slower at a balance task) may indicate an inability of animals to regulate their own locomotor speed during challenging conditions, perhaps because of disrupted motor efference copy information (9, 71, 72). This result also hints that the EVN normally acts to constrain movement speed, acting as a behavioral brake or stabilizer during dynamic motor tasks, possibly at the cost of long-term sensorimotor adaptability or precision. However, further behavioral assessment will be required to confirm this result.

One possible explanation for the limited behavioral effects observed could be the small number of cells ultimately affected by virally delivered manipulations. The EVN has few neurons, and only transducing a proportion of the cells within it results in a small overall intervention. Our CGRP-driven EVN targeting isolated on average 15 EVN neurons, approximately one-third of all EVN neurons, making it challenging for behavioral assays where a complete inhibition of the whole EVN would provide more clarity in results. In addition, given the highly plastic nature of the vestibular system and its ability to compensate for perturbations (75), the use of a chronic manipulation such as TeLC could obscure EVS function if the system were to compensate for this lack of output.

Limitations of Our Approach

The EVN is a very small brain nucleus containing only ~41 neurons per hemisphere in mice (18). Our technical approach requires up to four viruses to transduce the same neuron, in a brain region that is only a few hundred microns across. The result of this is that a small number of EVN neurons are targeted in our experiments. As discussed above, the small number of rabies starter neurons could provide only a partial picture of synaptic input. Similarly, the relatively small number of neurons targeted with TeLC could mean that the remaining, functional EVN can compensate for the loss of synaptic output from these neurons. As a result of this some behavioral roles of the EVN may be missed. Future refinements of this method should be targeted toward increasing its efficiency to complement the selectivity described here.

Conclusions and Next Steps

Here, we provide a novel means of targeting and accessing the EVN that we use for monosynaptic tracing of inputs and that could be applied to behavioral assessments of EVS function. Our input mapping experiments utilize rabies tracing methodology and provide valuable new information on the anatomical organization of the efferent vestibular system. For the first time, we present a map of the type of information that the EVN directly receives and processes. Combined with the existing body of EVS research, our findings highlight the dynamic, multimodal nature of the EVN, acting as a hub to integrate and update the vestibular periphery in real time with relevant internal and external information to support overall vestibular health.

Our molecular genetic strategy could also be used alongside bespoke behavioral tests to further demonstrate this filtering role or test alternative functional hypotheses. For example, head-fixed eye tracking for VOR performance or complex movement tasks, such as narrower or curved beam experiments, could be adapted to our technology. Our system is also compatible for use with acute circuit interventions such as chemo- or opto-genetics and calcium imaging, which could provide a clearer understanding of EVS function.

EVS research continues, and the novel methodology presented here could enable specific targeting of the EVN for functional research and, ultimately, faster progress in understanding this somewhat mysterious nucleus.

DATA AVAILABILITY

Data will be made available upon reasonable request.

SUPPLEMENTAL MATERIAL

Supplemental Tables S1 and S2 are available at: https://osf.io/8wz2g/files/osfstorage/6983745ad7eb2639cf4c4f46.

ACKNOWLEDGMENTS

The authors thank A. J. Camp for discussions and feedback on the projects in this publication. Mouse illustration in graphical abstract adapted from SciDraw by artists E. Tyler and L. Kravitz.

Present address of M. A. Mathews and A. J. Murray: Antelope Health Ltd., Millbank Tower, London, United Kingdom.

GRANTS

This work was supported by the Sainsbury Wellcome Centre core grant from the Gatsby Charitable Foundation (GAT3755) and the Wellcome Foundation (219627/Z/19/Z).

DISCLOSURES

No conflicts of interest, financial or otherwise, are declared by the authors.

AUTHOR CONTRIBUTIONS

M.A.M., V.W.K.T., and A.J.M. conceived and designed research; M.A.M. and V.W.K.T. performed experiments; M.A.M., V.W.K.T., E.C.R.-H., and A.J.M. analyzed data; M.A.M. prepared figures; M.A.M., V.W.K.T., E.C.R.-H., and A.J.M. drafted manuscript; M.A.M., V.W.K.T., E.C.R.-H., and A.J.M. edited and revised manuscript; M.A.M., V.W.K.T., E.C.R.-H., and A.J.M. approved final version of manuscript.

REFERENCES

1. **Hellmann B**, **Fritzsch B.** Neuroanatomical and histochemical evidence for the presence of common lateral line and inner ear efferents and of efferents to the basilar papilla in a frog, Xenopus laevis. *Brain Behav Evol* 47: 185–194, 1996. doi:10.1159/000113238.
2. **Mathews MA**, **Camp AJ**, **Murray AJ.** Reviewing the role of the efferent vestibular system in motor and vestibular circuits. *Front Physiol* 8: 552, 2017 [Erratum in *Front Physiol* 9: 687, 2018]. doi:10.3389/fphys.2017.00552.

3. **Holt JC**, **Lysakowski A**, **Goldberg JM.** The efferent vestibular system. In: *Auditory and Vestibular Efferents*, edited by Ryugo DK, Fay RR, Popper AN**.** Springer, 2010, p. 135–186.
4. **Raghu V**, **Salvi R**, **Sadeghi SG.** Efferent inputs are required for normal function of vestibular nerve afferents. *J Neurosci* 39: 0237, 2019. doi:10.1523/JNEUROSCI.0237-19.2019.
5. **Russell IJ.** The role of the lateral-line efferent system in Xenopus laevis. *J Exp Biol* 54: 621–641, 1971. doi:10.1242/jeb.54.3.621.
6. **Highstein SM**, **Baker R.** Action of the efferent vestibular system on primary afferents in the toadfish, Opsanus tau. *J Neurophysiol* 54: 370–384, 1985. doi:10.1152/jn.1985.54.2.370.
7. **Plotnik M**, **Marlinski V**, **Goldberg JM.** Reflections of efferent activity in rotational responses of chinchilla vestibular afferents. *J Neurophysiol* 88: 1234–1244, 2002. doi:10.1152/jn.2002.88.3.1234.
8. **Plotnik M**, **Marlinski V**, **Goldberg JM.** Efferent-mediated fluctuations in vestibular nerve discharge: a novel, positive-feedback mechanism of efferent control. *J Assoc Res Otolaryngol* 6: 311–323, 2005. doi:10.1007/s10162-005-0010-y.
9. **Chagnaud BP**, **Banchi R**, **Simmers J**, **Straka H.** Spinal corollary discharge modulates motion sensing during vertebrate locomotion. *Nat Commun* 6: 7982, 2015. doi:10.1038/ncomms8982.
10. **Luebke AE**, **Holt JC**, **Jordan PM**, **Wong YS**, **Caldwell JS**, **Cullen KE.** Loss of α-calcitonin gene-related peptide (αCGRP) reduces the efficacy of the Vestibulo-ocular Reflex (VOR). *J Neurosci* 34: 10453–10458, 2014. doi:10.1523/JNEUROSCI.3336-13.2014.
11. **Hübner PP**, **Khan SI**, **Migliaccio AA.** The mammalian efferent vestibular system plays a crucial role in the high-frequency response and short-term adaptation of the vestibuloocular reflex. *J Neurophysiol* 114: 3154–3165, 2015. doi:10.1152/jn.00307.2015.
12. **Hübner PP**, **Khan SI**, **Migliaccio AA.** The mammalian efferent vestibular system plays a crucial role in vestibulo-ocular reflex compensation after unilateral labyrinthectomy. *J Neurophysiol* 117: 1553–1568, 2017. doi:10.1152/jn.01049.2015.
13. **Chang HHV**, **Morley BJ**, **Cullen KE.** Loss of α-9 nicotinic acetylcholine receptor subunit predominantly results in impaired postural stability rather than gaze stability. *Front Cell Neurosci* 15: 799752, 2021. doi:10.3389/fncel.2021.799752.
14. **Mathews MA**, **Magnusson AK**, **Murray A**, **Camp AJ.** The efferent vestibular and octavolateralis system: anatomy, physiology and function. In: *The Senses: A Comprehensive Reference* (2nd ed.), edited by Fritzsch B**.** Academic Press, 2020, p. 512–525.
15. **Poppi LA**, **Holt JC**, **Lim R**, **Brichta AM.** A review of efferent cholinergic synaptic transmission in the vestibular periphery and its functional implications. *J Neurophysiol* 123: 608–629, 2020. doi:10.1152/jn.00053.2019.
16. **Cullen KE**, **Wei RH.** Differences in the structure and function of the vestibular efferent system among vertebrates. *Front Neurosci* 15: 684800, 2021. doi:10.3389/fnins.2021.684800.
17. **Leijon S**, **Magnusson AK.** Physiological characterization of vestibular efferent brainstem neurons using a transgenic mouse model. *PLoS One* 9: e98277, 2014. doi:10.1371/journal.pone.0098277.
18. **Mathews MA**, **Murray A**, **Wijesinghe R**, **Cullen K**, **Tung VW**, **Camp AJ.** Efferent vestibular neurons show homogenous discharge output but heterogeneous synaptic input profile in vitro. *PLoS One* 10: e0139548, 2015. doi:10.1371/journal.pone.0139548.
19. **Lorincz D**, **Poppi LA**, **Holt JC**, **Drury HR**, **Lim R**, **Brichta AM.** The long and winding road-vestibular efferent anatomy in mice. *Front Neural Circuits* 15: 751850, 2021. doi:10.3389/fncir.2021.751850.
20. **Watson A**, **Ensor E**, **Symes A**, **Winter J**, **Kendall G**, **Latchman D.** A Minimal CGRP gene promoter is inducible by nerve growth factor in adult rat dorsal root ganglion neurons but not in PC12 phaeochromocytoma cells. *Eur J Neurosci* 7: 394–400, 1995. doi:10.1111/j.1460-9568.1995.tb00335.x.
21. **Messina M**, **Yu DMT**, **Learoyd DL**, **Both GW**, **Molloy PL**, **Robinson BG.** High level, tissue-specific expression of a modified calcitonin/calcitonin gene-related peptide promoter in a human medullary thyroid carcinoma cell line. *Mol Cell Endocrinol* 164: 219–224, 2000. doi:10.1016/s0303-7207(00)00204-5.
22. **Durham PL**, **Dong PX**, **Belasco KT**, **Kasperski J**, **Gierasch WW**, **Edvinsson L**, **Heistad DD**, **Faraci FM**, **Russo AF.** Neuronal expression and regulation of CGRP promoter activity following viral gene transfer into cultured trigeminal ganglia neurons. *Brain Res* 997: 103–110, 2004. doi:10.1016/j.brainres.2003.11.005.
23. **Shimizu N**, **Doyal MF**, **Goins WG**, **Kadekawa K**, **Wada N**, **Kanai AJ**, **de Groat WC**, **Hirayama A**, **Uemura H**, **Glorioso JC**, **Yoshimura N.** Morphological changes in different populations of bladder afferent neurons detected by herpes simplex virus (HSV) vectors with cell-type-specific promoters in mice with spinal cord injury. *Neuroscience* 364: 190–201, 2017 [Erratum in *Neuroscience* 381: 161, 2018]. doi:10.1016/j.neuroscience.2017.09.024.
24. **Ohno K**, **Takeda N**, **Yamano M**, **Matsunaga T**, **Tohyama M.** Coexistence of acetylcholine and calcitonin gene-related peptide in the vestibular efferent neurons in the rat. *Brain Res* 566: 103–107, 1991. doi:10.1016/0006-8993(91)91686-u.
25. **Thomas PM**, **Nasonkin I**, **Zhang H**, **Gagel RF**, **Cote GJ.** Structure of the mouse calcitonin/calcitonin gene-related peptide alpha and beta genes. *DNA Seq* 12: 131–135, 2001. doi:10.3109/10425170109047567.
26. **Murray AJ**, **Sauer JF**, **Riedel G**, **Mcclure C**, **Ansel L**, **Cheyne L**, **Bartos M**, **Wisden W**, **Wulff P.** Parvalbumin-positive CA1 interneurons are required for spatial working but not for reference memory. *Nat Neurosci* 14: 297–299, 2011. doi:10.1038/nn.2751.
27. **McClure C**, **Cole KL**, **Wulff P**, **Klugmann M**, **Murray AJ.** Production and titering of recombinant adeno-associated viral vectors. *J Vis Exp* 57: e3348, 2011. doi:10.3791/3348.
28. **Reardon TR**, **Murray AJ**, **Turi GF**, **Wirblich C**, **Croce KR**, **Schnell MJ**, **Jessell TM**, **Losonczy A.** Rabies virus CVS-N2c(ΔG) strain enhances retrograde synaptic transfer and neuronal viability. *Neuron* 89: 711–724, 2016. doi:10.1016/j.neuron.2016.01.004.
29. **Rossi J**, **Balthasar N**, **Olson D**, **Scott M**, **Berglund E**, **Lee CE**, **Choi MJ**, **Lauzon D**, **Lowell BB**, **Elmquist JK.** Melanocortin-4 receptors expressed by cholinergic neurons regulate energy balance and glucose homeostasis. *Cell Metab* 13: 195–204, 2011. doi:10.1016/j.cmet.2011.01.010.
30. **Madisen L**, **Zwingman TA**, **Sunkin SM**, **Oh SW**, **Zariwala HA**, **Gu H**, **Ng LL**, **Palmiter RD**, **Hawrylycz MJ**, **Jones AR**, **Lein ES**, **Zeng H.** A robust and high-throughput Cre reporting and characterization system for the whole mouse brain. *Nat Neurosci* 13: 133–140, 2010. doi:10.1038/nn.2467.
31. **Cetin A**, **Komai S**, **Eliava M**, **Seeburg PH**, **Osten P.** Stereotaxic gene delivery in the rodent brain. *Nat Protoc* 1: 3166–3173, 2006. doi:10.1038/nprot.2006.450.
32. **Yates SC**, **Groeneboom NE**, **Coello C**, **Lichtenthaler SF**, **Kuhn PH**, **Demuth HU**, **Hartlage-Rübsamen M**, **Roßner S**, **Leergaard T**, **Kreshuk A**, **Puchades MA**, **Bjaalie JG.** QUINT: workflow for quantification and spatial analysis of features in histological images from rodent brain. *Front Neuroinform* 13: 75, 2019. doi:10.3389/fninf.2019.00075.
33. **Tung VW**, **Burton TJ**, **Dababneh E**, **Quail SL**, **Camp AJ.** Behavioral assessment of the aging mouse vestibular system. *J Vis Exp* 11: 51605, 2014. doi:10.3791/51605.
34. **Schutz H**, **Jamniczky HA**, **Hallgrímsson B**, **Garland T Jr.** Shape-shift: semicircular canal morphology responds to selective breeding for increased locomotor activity. *Evolution* 68: 3184–3198, 2014. doi:10.1111/evo.12501.
35. **Nectow AR**, **Nestler EJ.** Viral tools for neuroscience. *Nat Rev Neurosci* 21: 669–681, 2020. doi:10.1038/s41583-020-00382-z.
36. **Hardisty-Hughes RE**, **Parker A**, **Brown SD.** A hearing and vestibular phenotyping pipeline to identify mouse mutants with hearing impairment. *Nat Protoc* 5: 177–190, 2010. doi:10.1038/nprot.2009.204.
37. **Rogers A**, **Beier KT.** Can transsynaptic viral strategies be used to reveal functional aspects of neural circuitry? *J Neurosci Methods* 348: 109005, 2021. doi:10.1016/j.jneumeth.2020.109005.
38. **Tran-Van-Minh A**, **Ye Z**, **Rancz E.** Quantitative analysis of rabies virus-based synaptic connectivity tracing. *PLoS One* 18: e0278053, 2023. doi:10.1371/journal.pone.0278053.
39. **Metts BA**, **Kaufman GD**, **Perachio AA.** Polysynaptic inputs to vestibular efferent neurons as revealed by viral transneuronal tracing. *Exp Brain Res* 172: 261–274, 2006. doi:10.1007/s00221-005-0328-z.
40. **Zhou YJ**, **Zhao H**, **Wang Y**, **Yu J**, **Tian L**, **Wang J.** Stimulation or lesion of the medial vestibular nucleus increases the number of choline acetyltransferase-positive efferent vestibular neurons in the brainstem. *Neuroreport* 29: 1315–1322, 2018. doi:10.1097/WNR.0000000000001115.
41. **Dietrich H**, **Glasauer S**, **Straka H.** Functional organization of vestibulo-ocular responses in abducens motoneurons. *J Neurosci* 37: 4032–4045, 2017. doi:10.1523/JNEUROSCI.2626-16.2017.

42. **McFarland JL**, **Fuchs AF.** Discharge patterns in nucleus prepositus hypoglossi and adjacent medial vestibular nucleus during horizontal eye movement in behaving macaques. *J Neurophysiol* 68: 319–332, 1992. doi:10.1152/jn.1992.68.1.319.
43. **Mettens P**, **Godaux E**, **Cheron G**, **Galiana HL.** Effect of muscimol microinjections into the prepositus hypoglossi and the medial vestibular nuclei on cat eye movements. *J Neurophysiol* 72: 785–802, 1994. doi:10.1152/jn.1994.72.2.785.
44. **Müri RM**, **Chermann JF**, **Cohen L**, **Rivaud S**, **Pierrot-Deseilligny C.** Ocular motor consequences of damage to the abducens nucleus area in humans. *J Neuroophthalmol* 16: 191–195, 1996.
45. **Lisberger SG**, **Miles FA.** Role of primate medial vestibular nucleus in long-term adaptive plasticity of vestibuloocular reflex. *J Neurophysiol* 43: 1725–1745, 1980. doi:10.1152/jn.1980.43.6.1725.
46. **Goldberg JM**, **Fernández C.** Efferent vestibular system in the squirrel monkey: anatomical location and influence on afferent activity. *J Neurophysiol* 43: 986–1025, 1980. doi:10.1152/jn.1980.43.4.986.
47. **Highstein SM.** The central nervous system efferent control of the organs of balance and equilibrium. *Neurosci Res* 12: 13–30, 1991. doi:10.1016/0168-0102(91)90096-h.
48. **Brichta AM**, **Goldberg JM.** Responses to efferent activation and excitatory response-intensity relations of turtle posterior-crista afferents. *J Neurophysiol* 83: 1224–1242, 2000. doi:10.1152/jn.2000.83.3.1224.
49. **Elgoyhen AB**, **Johnson DS**, **Boulter J**, **Vetter DE**, **Heinemann S.** Alpha 9: an acetylcholine receptor with novel pharmacological properties expressed in rat cochlear hair cells. *Cell* 79: 705–715, 1994. doi:10.1016/0092-8674(94)90555-x.
50. **Hiel H**, **Elgoyhen AB**, **Drescher DG**, **Morley BJ.** Expression of nicotinic acetylcholine receptor mRNA in the adult rat peripheral vestibular system. *Brain Res* 738: 347–352, 1996. doi:10.1016/s0006-8993(96)01046-3.
51. **Anderson AD**, **Troyanovskaya M**, **Wackym PA.** Differential expression of alpha2-7, alpha9 and beta2-4 nicotinic acetylcholine receptor subunit mRNA in the vestibular end-organs and Scarpa's ganglia of the rat. *Brain Res* 778: 409–413, 1997. doi:10.1016/s0006-8993(97)01121-9.
52. **Holt JC**, **Jordan PM**, **Lysakowski A**, **Shah A**, **Barsz K**, **Contini D.** Muscarinic acetylcholine receptors and M-currents underlie efferent-mediated slow excitation in calyx-bearing vestibular afferents. *J Neurosci* 37: 1873–1887, 2017. doi:10.1523/JNEUROSCI.2322-16.2017.
53. **Zhou T**, **Wang Y**, **Guo CK**, **Zhang WJ**, **Yu H**, **Zhang K**, **Kong WJ.** Two distinct channels mediated by m2mAChR and α9nAChR coexist in type II vestibular hair cells of guinea pig. *Int J Mol Sci* 14: 8818–8831, 2013. doi:10.3390/ijms14058818.
54. **Xiaocheng W**, **Zhaohui S**, **Junhui X**, **Lei Z**, **Lining F**, **Zuoming Z.** Expression of calcitonin gene-related peptide in efferent vestibular system and vestibular nucleus in rats with motion sickness. *PLoS One* 7: e47308, 2012. doi:10.1371/journal.pone.0047308.
55. **Tu L**, **Poppi L**, **Rudd J**, **Cresswell ET**, **Smith DW**, **Brichta A**, **Nalivaiko E.** Alpha-9 nicotinic acetylcholine receptors mediate hypothermic responses elicited by provocative motion in mice. *Physiol Behav* 174: 114–119, 2017. doi:10.1016/j.physbeh.2017.03.012.
56. **Lorincz D**, **Drury HR**, **Smith DW**, **Lim R**, **Brichta AM.** Aged mice are less susceptible to motion sickness and show decreased efferent vestibular activity compared to young adults. *Brain Behav* 13: e3064, 2023. doi:10.1002/brb3.3064.
57. **Boissard R**, **Fort P**, **Gervasoni D**, **Barbagli B**, **Luppi PH.** Localization of the GABAergic and non-GABAergic neurons projecting to the sublaterodorsal nucleus and potentially gating paradoxical sleep onset. *Eur J Neurosci* 18: 1627–1639, 2003. doi:10.1046/j.1460-9568.2003.02861.x.
58. **Fraigne JJ**, **Torontali ZA**, **Snow MB**, **Peever JH.** REM sleep at its core–circuits, neurotransmitters, and pathophysiology. *Front Neurol* 6: 123, 2015. doi:10.3389/fneur.2015.00123.
59. **Ryan PJ**, **Ma S**, **Olucha-Bordonau FE**, **Gundlach AL.** Nucleus incertus—an emerging modulatory role in arousal, stress and memory. *Neurosci Biobehav Rev* 35: 1326–1341, 2011. doi:10.1016/j.neubiorev.2011.02.004.
60. **Valencia Garcia S**, **Libourel PA**, **Lazarus M**, **Grassi D**, **Luppi PH**, **Fort P.** Genetic inactivation of glutamate neurons in the rat sublaterodorsal tegmental nucleus recapitulates REM sleep behaviour disorder. *Brain* 140: 414–428, 2017. doi:10.1093/brain/aww310.
61. **Andresen MC**, **Paton JF.** The nucleus of the solitary tract: processing information from viscerosensory afferents. In: *Central Regulation of Autonomic Functions*, edited by Ida J. Llewellyn-Smith, Anthony J. M. Verberne. Oxford University Press, 2011, vol. 2, p. 23–46.
62. **Zoccal DB**, **Furuya WI**, **Bassi M**, **Colombari DS**, **Colombari E.** The nucleus of the solitary tract and the coordination of respiratory and sympathetic activities. *Front Physiol* 5: 238, 2014. doi:10.3389/fphys.2014.00238.
63. **Biazoli CE Jr**, **Goto M**, **Campos AMP**, **Canteras NS.** The supragenual nucleus: a putative relay station for ascending vestibular signs to head direction cells. *Brain Res* 1094: 138–148, 2006. doi:10.1016/j.brainres.2006.03.101.
64. **Xiao C**, **Wei J**, **Zhang G-W**, **Tao C**, **Huang JJ**, **Shen L**, **Wickersham IR**, **Tao HW**, **Zhang LI.** Glutamatergic and GABAergic neurons in pontine central gray mediate opposing valence-specific behaviors through a global network. *Neuron* 111: 1486–1503.e7, 2023. doi:10.1016/j.neuron.2023.02.012.
65. **Lim SB**, **Cleworth TW**, **Horslen BC**, **Blouin JS**, **Inglis JT**, **Carpenter MG.** Postural threat influences vestibular-evoked muscular responses. *J Neurophysiol* 117: 604–611, 2017. doi:10.1152/jn.00712.2016.
66. **Naranjo EN**, **Cleworth TW**, **Allum JHJ**, **Inglis JT**, **Lea J**, **Westerberg BD**, **Carpenter MG.** Vestibulo-spinal and vestibulo-ocular reflexes are modulated when standing with increased postural threat. *J Neurophysiol* 115: 833–842, 2016. doi:10.1152/jn.00626.2015.
67. **Münz H**, **Claas B.** Activity of lateral line efferents in the axolotl (Ambystoma mexicanum). *J Comp Physiol A* 169: 461–469, 1991. doi:10.1007/BF00197658.
68. **Roberts BL**, **Russell IJ.** The activity of lateral-line efferent neurones in stationary and swimming dogfish. *J Exp Biol* 57: 435–448, 1972. doi:10.1242/jeb.57.2.435.
69. **Witts EC**, **Murray AJ.** Vestibulospinal contributions to mammalian locomotion. *Curr Opin Physiol* 8: 56–62, 2019. doi:10.1016/j.cophys.2018.12.010.
70. **Takakusaki K**, **Chiba R**, **Nozu T**, **Okumura T.** Brainstem control of locomotion and muscle tone with special reference to the role of the mesopontine tegmentum and medullary reticulospinal systems. *J Neural Transm (Vienna)* 123: 695–729, 2016. doi:10.1007/s00702-015-1475-4.
71. **Lunsford ET**, **Skandalis DA**, **Liao JC.** Efferent modulation of spontaneous lateral line activity during and after zebrafish motor commands. *J Neurophysiol* 122: 2438–2448, 2019. doi:10.1152/jn.00594.2019.
72. **Odstrcil I**, **Petkova MD**, **Haesemeyer M**, **Boulanger-Weill J**, **Nikitchenko M**, **Gagnon JA**, **Oteiza P**, **Schalek R**, **Peleg A**, **Portugues R**, **Lichtman JW**, **Engert F.** Functional and ultrastructural analysis of reafferent mechanosensation in larval zebrafish. *Curr Biol* 32: 176–189.e5, 2022. doi:10.1016/j.cub.2021.11.007.
73. **Pichler P**, **Lagnado L.** Motor behavior selectively inhibits hair cells activated by forward motion in the lateral line of zebrafish. *Curr Biol* 30: 150–157.e3, 2020. doi:10.1016/j.cub.2019.11.020.
74. **Tung VW**, **Burton TJ**, **Quail SL**, **Mathews MA**, **Camp AJ.** Motor performance is impaired following vestibular stimulation in ageing mice. *Front Aging Neurosci* 8: 12, 2016. doi:10.3389/fnagi.2016.00012.
75. **Gittis AH**, **Du Lac S.** Intrinsic and synaptic plasticity in the vestibular system. *Curr Opin Neurobiol* 16: 385–390, 2006. doi:10.1016/j.conb.2006.06.012.